Sustainable Energy Technologies and Assessments 57 (2023) 103297

Contents lists available at ScienceDirect

Sustainable Energy Technologies and Assessments

journal homepage: www.elsevier.com/locate/seta

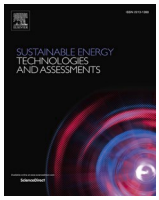

Original article

Hydrogen based configurations for an overhead crane with quasi-Z-source inverter

Pablo García-Triviño [a], Raúl Sarrias-Mena [b], Carlos Andrés García-Vázquez [a], Francisco Llorens-Iborra [a], Higinio Sánchez-Sainz [c], Luis M. Fernández-Ramírez [a,*]

[a] Research Group in Sustainable and Renewable Electrical Technologies (PAIDI-TEP-023), Department of Electrical Engineering, EPS Algeciras, University of Cadiz, Avda. Ramón Puyol, s/n, 11202 Algeciras (Cádiz), Spain
[b] Research Group in Sustainable and Renewable Electrical Technologies (PAIDI-TEP-023), Department of Engineering in Automation, Electronics and Computer Architecture & Networks, EPS Algeciras, University of Cadiz, Avda. Ramón Puyol, s/n, 11202 Algeciras (Cádiz), Spain
[c] Research Group in Sustainable and Renewable Electrical Technologies (PAIDI-TEP-023), Department of Electrical Engineering, ESI Puerto Real, University of Cádiz, Avda. Universidad de Cádiz, n°10, 11519 Puerto Real (Cádiz), Spain

ARTICLE INFO

Keywords:
Crane
Hydrogen
Fuel cell
Electrolyzer
Energy storage system
Quasi-Z-source inverter

ABSTRACT

Most of the overhead cranes used to date are powered by diesel engine or electrical grid and voltage source inverter. The economic and environmental costs of fossil fuels, and the unsteady price of electricity, encourage exploring new applications for developing electric power technologies. In this scenario, the main objective of this paper is to analyze the technical and economic feasibility of two new configurations based on hydrogen system and quasi-Z-source inverter (qZSI) for an overhead crane. The first configuration uses a fuel cell (FC) connected to a qZSI to supply the crane. The second one integrates an electrolyzer (LZ) as an energy storage system (ESS) into the impedance network of the qZSI (without additional DC/DC converter), which allows to recover energy during the regenerative braking of the crane and use it to produce hydrogen. The modelling and control are described, and short simulations of the working cycle of the crane under different initial hydrogen tank levels, and long simulations with several working cycles, are considered. The results show the technical viability of the two hydrogen-based configurations and the control systems implemented, since they can power the crane under all the situations studied. Nevertheless, the configuration with FC and LZ presents a higher energy efficiency (65% vs 44% with the FC-only configuration). Regarding the economic study, both configurations are compared with a diesel-based and with a full-electric configuration powered by the grid. Analyzing both hydrogen-based configurations, the results show that the configuration with FC and FZ becomes more profitable after 1.56 years, despite the higher initial cost. However, both configurations result more expensive than those based on diesel engine and fully powered by the grid. The two proposed configurations would be more cost-effective than the initial configuration in a plausible future with a 40% decrease in hydrogen cost.

Introduction

The global crisis in the energy market is affecting the cost of fossil fuels, and this is harming consumers severely. The rise in the price of fuels in 2022 is responsible for 90% of the increase in the average costs of electricity generation worldwide, with natural gas contributing with more than 50% [1]. On the other hand, renewable energy generation, led by wind and solar power, increased around 17% in 2021, meaning over a half of the global power generation increase during 2020–21 [2]. Therefore, developing the less mature renewable energy technologies, promoting energy storage, and introducing clean technologies to new applications is more necessary than ever before. Over the last years, hydrogen energy has become a reality in new energy systems. It can be produced from renewable sources, as well as, transported and stored [3], and it is suitable for emission-free electricity generation with low environmental impact [4]. In this sense, recent research has revealed that hydrogen production from wind power has a lower global warming potential than other alternatives presented in the literature [A review on global warming potential, challenges and opportunities of renewable hydrogen production technologies]. Energy production, transport and heating for buildings and industry are the main areas where hydrogen

* Corresponding author.
E-mail addresses: pablo.garcia@uca.es (P. García-Triviño), raul.sarrias@uca.es (R. Sarrias-Mena), carlosandres.garcia@uca.es (C.A. García-Vázquez), francisco.llorens@uca.es (F. Llorens-Iborra), higinio.sanchez@uca.es (H. Sánchez-Sainz), luis.fernandez@uca.es (L.M. Fernández-Ramírez).

https://doi.org/10.1016/j.seta.2023.103297
Received 10 October 2022; Received in revised form 13 March 2023; Accepted 20 May 2023
Available online 28 May 2023

Nomenclature

2. Hydrogen based configuration

V_{dc} Output voltage of the qZSI impedance network

2.3 Power control

FC and LZ Fuel cell and electrolyzer

D Shoot-though period

Do and ΔD Control term for D

$I_{d,AC}$ and $I_{q,AC}$ Grid current reference (dq frame)

M and m_{abc} Modulation index and modulation signal

m_d and m_q dq components of the modulation index

P_{LZ}^{ref} Reference LZ power

u_d and u_q Grid voltage (dq frame)

V_{FC}^{nom} and V_{LZ}^{nom} Fuel cell and electrolyzer nominal voltage

T_{sh} Shoot-through state

T_s Sample time

4. Results and Discussion

C_{ac} Acquisition cost of the crane

C_{die} and C_{H2} Diesel cost in € per litre and H_2 cost in € per kg

C_{grid} and C_{iny} Cost of the energy absorbed from and injected into the grid

C_t Net cash flow

$Cost$ Total utilization cost of the crane

E_{abs}^{cycle} and E_{gen}^{cycle} Energy absorbed and generated by the system in each configuration

IRR Internal return ratio

L_{H2} and L_{H2}^{min} Current and minimum hydrogen tank level

$N_{cycle}, N_{cycle,y}$ and N_{year} Working cycles, working cycle of the crane in a year and working years of the crane

P_{FC}^{max} and P_{FC}^{nom} Maximum (depend on L_{H2}) and nominal FC power

Q_{H2}^{cycle} and Q_{die}^{kWh} H_2 consumption in a cycle and diesel consumption per unit of energy

Appendix B. Modelling of the components

N_{FC} and N_{stack} Number of FC and number of stacks

$N_{s,LZ}$ and $N_{p,LZ}$ Number of LZ in series and in parallel

CAP_{H2} Hydrogen tank capacity

k_p and k_i Constants of the PI controllers

P_{LZ}^{nom} LZ nominal power

B.1. Fuel cell

C_p Air specific heat capacity

E_{cell} and E_{cell}^0 Nernst's instantaneous voltage and standard-state reversible voltage

k_e Function of the entropy change

M_v, M_a and M_{O2} Molar masses of water, dry air, and oxygen

p_{cat}, p_{atm} and p_{sat} Cathode, atmospheric and saturation pressure

p_{H2}, p_{H2o} and p_{o2} Partial pressures of water, hydrogen and oxygen

q_{H2}^r, q_{O2}^r and q_{air} Amount of hydrogen and oxygen reacting in the anode and cathode of the FC, and input air flow

R and F Ideal gas constant and Faraday's constant

T and T_{ref} Working operation temperature of the FC and reference temperature

V_{act} and V_{ohm} Activation and ohmic voltages

V_{FC} FC voltage

V_{irrev} Irreversible FC voltage

x_{O2} Oxygen mass fraction in air

γ Ratio of the specific heat of air

η_{com} Compressor efficiency

λ_{O2} Ratio between the input and the consumed oxygen in the FC

B.2. Electrolyzer

e_{rev} Reverse voltage

p and p_0 Current and reference pressure in the LZ

q_{H2}^{pro} and q_{H2}^{con} H_2 production and consumption

R_i, R_{i0} and R_t Internal resistance, reference internal resistance and variation of the LZ internal resistance

V_{rev} and V_{rev0} Minimum voltage in the LZ needed to produce a current flow and reference value for the reverse voltage

B.3. Simplified model of the quasi-Z-source inverter

B Voltage gain between the input and the output of the impedance network

I_{in} Input current to the impedance network

I_a, I_b and I_c Currents in the AC side of the inverter

I_d and I_q Currents in the AC side of the inverter (dq frame)

P_{grid} and P_{in} Grid and input power to the impedance network

V_a, V_b and V_c Voltages in the AC side of the inverter

V_{in} and V_{C2} Input voltage to the impedance network and voltage in the capacitor C2

V_d and V_q Voltages in the AC side of the inverter

can emerge as a low-carbon option [5].

Hydrogen FC has higher efficiency compared to other power sources. It is non-polluting, having water, instead of CO_2, as the main by-product. Besides, the absence of moving parts reduces its maintenance requirements, and the noise during operation [6]. Among all the FC available in the market, Proton Exchange Membrane Fuel Cell (PEM-FC) is the most widely used in the existing literature.

FC are mainly applied to FC-vehicles and FC-based power systems, replacing the conventional internal combustion engines (ICE). Not only road transportation, but also marine vessels or aviation systems are working towards FC propulsion in a commercial scale [7]. In applications with road vehicles, FC are used together with other energy storage devices, such as supercapacitors (SC) or batteries. In [8], powertrains based on battery electric vehicles and FC vehicles were studied as a means of decarbonising the transport sector. A hybrid vehicle configuration with battery and FC was presented in [9], where the authors evaluated the optimal battery capacity and FC-to-battery energy distribution ratio under different load profiles. In [10], the FC was the power main source, while the battery and the SC acted as back-up storage systems for a tramway, in order to provide fastest dynamic response and absorb the power generated during braking. FC-vehicle was also used in [11], but in this case with a solar-hydrogen mild hybrid configuration. Authors in [12] considered the hybridization of a FC and batteries for a ferry, and proposed a methodology to study the feasibility and potential benefit of the propulsion system. In FC-based power system applications, the works published in the literature mainly focused on integrating FC into hybrid renewable energy systems (HRES) in microgrids, with wind turbines and solar photovoltaic panels as main sources of the system, and energy storage devices such as battery, SC, and hydrogen system as back-up energy sources [13,14,15,16,17]. In these cases, the hydrogen system is composed of FC, hydrogen tank and LZ. Such configuration provides much flexibility, as electricity and hydrogen can be consumed and generated on demand [18]. The LZ uses the surplus power in the microgrid, during overgeneration of renewable sources, to generate hydrogen that can be stored or supplied to hydrogen consumers using natural gas infrastructure [17]. Among other feasible applications, the hydrogen produced can be used in the FC to generate electricity when the renewable generation does not meet consumption. Using renewable energy for hydrogen production contributes to the decarbonization of electric power generation, as well as many other sectors [19]. The most

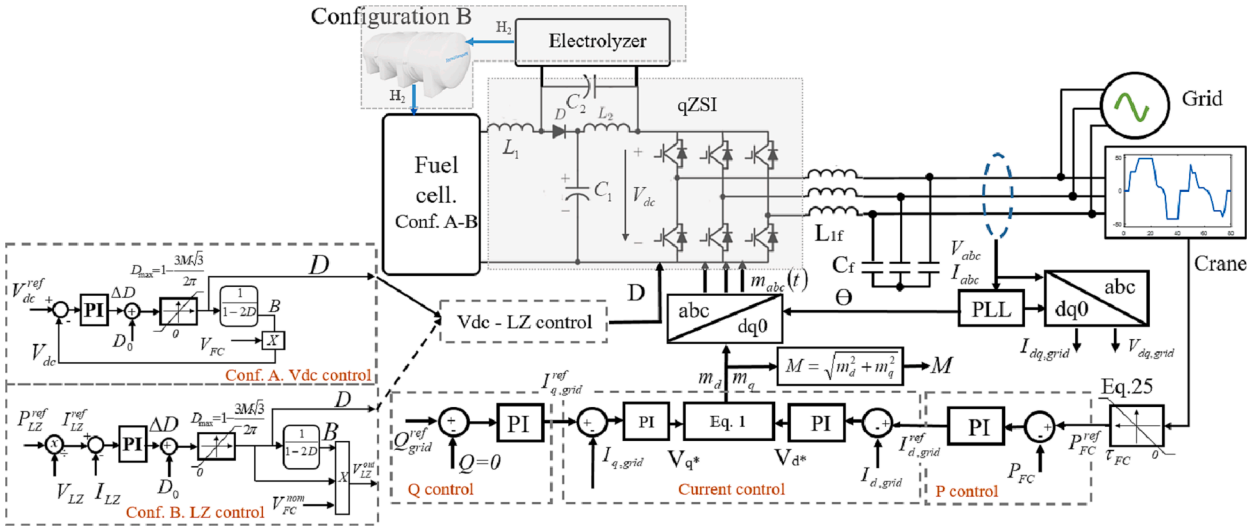

Fig. 1. Configurations and control of the crane.

promising hydrogen production technologies for such purposes are reviewed in [20].

The optimal sizing of a HRES was presented in [13]. A new power management system to integrate the power output from photovoltaic panel, FC, battery and a provision for onsite hydrogen generation by means of an LZ and hydrogen tank was presented in [14]. A new mathematical model of HRES was developed in [15] for the prediction of the charging/discharging characteristics of hydrogen storage units with renewable sources. A hybrid refuelling/power charging station for electric vehicles and FC was presented in [16]. The system was composed of PV system and hydrogen system.

Power converters in systems with FC are the key to achieve an optimal energy management, as well as an adequate stability in the DC voltage links [21]. FC and LZ do not admit current in the reverse direction, thus unidirectional DC-DC converters are needed to maintain the DC voltage properly regulated. Furthermore, in most of the applications, a voltage source inverter is required to convert DC voltage into AC for end-users, or for energy transport and distribution into other grids [6]. The conventional configuration is structured on a dual-stage conversion, which involves a DC-DC boost converter plus a DC-AC voltage source inverter. This topology has been thoroughly studied in the literature. A review of FC-grid interface was carried out in [22]. New topologies can be considered in order to minimize FC power conditioning, replacing the conventional two-stage converter to one-stage converter, such as Z-source inverters (ZSI) [23]. Thus, ZSI are a promising alternative due to their reliability, their robustness, and reduced costs. Quasi-ZSI (qZSI) is one of the most attractive ZSI topology due to continuous input current, stress reduction on the components and the simplicity of its control. The main field of research about ZSI are photovoltaic systems, but there are a few studies using a FC as the primary power source. The dynamic response of a FC with a ZSI controller connected to a 3-phase load was studied in [24]. Maximum constant boost control for a qZSI connected to a FC system was proposed in [25]. A FC power plant with a qZSI was described in [26] to enhance the efficiency of the power conditioning system. On the other hand, a FC with a modified qZSI was applied in [27] to a three-phase motor drive.

Cranes, powered by diesel engine or electricity, play a critical role in transportation (such as rubber tyre gantry (RTG) container crane, or rail mounted gantry (RMG) crane) and industry (such as overhead crane) [28]. Their energy consumption causes high and fluctuating costs. Subsequently, a reduction of their energy consumption becomes vital to keep these costs contained and search for a profitable operation of this machinery. At the same time, they help towards a greener future [29]. In this sense, Energy Storage Systems (ESSs) such as batteries, SCs, or flywheels, can help increasing the efficiency of the system when integrated into hybrid powertrains [30]. Hybridization of RTG cranes was studied in [31]. In this work, several ESSs were compared with the aim of recovering energy from the working cycle of the crane and investigating the cost-effectiveness of the proposed solutions. The results reflected that fuel saving up to 60% can be achieved. A review of technical solutions for the power supply of RTG cranes with hybrid energy storage systems was presented in [32]. The peak power demand issues in electrical cranes were addressed in [28]. In this case, two different technologies were compared, considering their potential for energy savings through reuse in RTG cranes. The first case presented an ESS, whereas the second used an active front-end converter, connected to the DC bus of the inverter. Both schemes allowed the reuse of the energy generated by the hoist motor of the crane. They concluded that the ESS system is more efficient, but the converter could help reduce the primary energy demand. In general, it can be stated that electric and hybrid RTG are feasible solutions [33–41]. A RTG container crane powered by a hybrid system comprising a diesel generator and SCs was studied in [33]. Hybridization with batteries of a low voltage network for electrical RTG cranes was presented in [34]. Owing to the batteries, the results indicated cost savings, peak demand reduction, and better performance of the network. A RTG crane powered by a battery-SC hybrid source was proposed in [35]. The load profile of the crane was studied to size the ESS, and the power flow was regulated through a state machine. The main drawback of the system was the high initial cost caused by the power converter of the SC. The adequacy of ESS in electrified RTG cranes equipped with hybrid power systems was investigated in [36]. Compared with a traditional crane, the electrified cranes can recover energy through regeneration, which reduces costs, fuel consumption and emissions. A grid-connected RTG crane with a battery ESS was studied in [37], where an energy management system was proposed that achieved a cost reduction of approximately 65% and a reduction in the peak power demand. Reference [38] deals with a RTG crane powered by a hybrid system comprising a diesel generator, battery, and SC. This work developed a novel energy management system that allowed maintaining the state of charge of the battery through a smart regulation of the power flows. As a result, the battery lifetime could be enhanced, with reduced fuel consumption compared to the conventional system. An energy management system based on game theory was proposed in [39] for a RTG crane powered by a diesel generator, battery and SC. This control scheme increased the energy efficiency of the system and improved the economy of the crane. After studying three different scenarios, they concluded that the combination of these components allowed addressing the power demand, provided a satisfactory

Table 1
Power control on each configuration.

	Config. A (without LZ)	Config. B (with LZ)
Load demand	FC. Grid if no hydrogen.	FC. Grid if no hydrogen.
Regenerative power	Injected into the grid or burnt in the braking resistor	Absorbed by the LZ, injected into the grid or burnt in the braking resistor
DC voltage (V_{dc})	Reference value set to 1500 V	It changes depending on the D
AC voltage	Controlled by the grid	Controlled by the grid

performance, reduced fuel consumption and cut down the emissions. Flywheel energy storage was considered as ESS in [40] to exploit the energy harvested from the electrical-powered crane. As a result, with the proposed control strategy, the ESS maintained the supply quality and enhanced the energy efficiency of the whole power system. Far from diesel-engine or electrified power system. A new "full green" FC and SC hybrid propulsion system was proposed and evaluated under the actual operation cycle of a RTG crane in [41]. The results demonstrated the technical viability, although it was more expensive.

This paper presents two new powertrain configurations based on hydrogen system and qZSI for an industrial overhead crane. The difference between each configuration is based on the integration of an LZ into the qZSI, which is working as ESS to recover energy during regenerative braking. Therefore, the main innovation points of this work are the following:

(1) The use of a FC as primary source to power an overhead crane.
(2) The use of an LZ as ESS to recover wasted energy during braking in the crane operation cycle and produce hydrogen.
(3) The incorporation of a qZSI as single-stage power converter instead of the traditional configuration based on a DC-DC boost converter and a three-phase voltage source inverter.
(4) The development of a simplified model of the qZSI, integrating the LZ in the second configuration.
(5) The analysis of the techno-economic viability of the proposed configurations, and the comparison with the configurations based on diesel engine and fully powered by the grid.

Data and methodology

Hydrogen-based configurations

The machine considered herein consists of an overhead crane usually installed in industrial buildings or warehouses. A typical crane cycle without considering the gantry maneuver is illustrated in Appendix A.

Fig. 1 shows the new configurations proposed for powering the overhead crane. They are based on hydrogen systems. In one of them, configuration A, the main energy source is a 50 kW PEM-FC, while in the second proposal, configuration B, a 80 kW LZ has also been added. Thus, in the configuration B, the available power during braking will be used to produce hydrogen, and besides, conversely to what happens in the current configuration, the option of injecting energy to the grid has been considered.

On the other hand, a qZSI has been selected for the connection of the FC and LZ. This kind of power converter allows adapting properly the output voltage of these new elements to the voltage of the current motors, and controls the power flows using a minimum number of power switches. It can be observed in Fig. 1 that the FC is connected to the input of the qZSI (input to the impedance network), while in the configuration B, the LZ is connected in parallel to the capacitor C2. The output voltage of the impedance network is defined as V_{dc}.

Modelling

The power control and the modelling of the qZSI differ depending on the proposed configuration. The modelling of the components and the most representative parameters for both configurations are described in Appendix B.

Power control

In the two new configurations presented herein, the main energy supply for the crane is provided by the FC. Subsequently, this device has to generate the load demand (positive values in Fig. 1). Nevertheless, during a descent or braking, the demanded power is transformed into available power. In the configuration A, this power has to be burnt or absorbed by the grid. Nevertheless, in the configuration B, this available power can be absorbed by the LZ. This power is used to produce hydrogen and, thus, extend the use of the hydrogen stored in the tank. In both cases, the grid is responsible for regulating the AC voltage. Table 1 summarizes the operation of each configuration.

The control strategies used for both configurations are explained below. The use of proper modulation techniques is essential to regulate the power flow in the crane. Currently, there are several modulation techniques applicable to a qZSI. Within the family of space-vector modulation techniques for ZSI (ZSVM), several options arise which differ on their switching patterns, such as ZSVM6, ZSVM4, ZSVM2 and ZSVM1 [42,43]. For the current work, the ZSVM6 technique has been used. This technique has two main advantages over the rest: 1) it allows a higher voltage gain, and 2) it reduces the voltage stress in the elements of the qZSI for the same voltage gain.

The conventional SVM presents six active states and two zero states, thus generating eight space vectors. The ZSVM adds one additional state, known as the shoot-through state (T_{sh}), in which one or more of the inverter legs are short-circuited. Thus, the shoot-though period (D) is defined as T_{sh}/T_s, where T_s in the sample time. In addition to D, the qZSI is also controlled through the modulation signal m_{abc}, which is a balanced three-phase signal. If it is transformed to the dq frame and its module is calculated, the modulation index M can be obtained. Fig. 1 shows the control loops implemented to control the output power of the FC (modifying M; m_{abc}). Furthermore, Fig. 1 depicts the control strategies developed for controlling V_{dc} through D in the configuration without LZ (Vdc loop control in Fig. 1), and the power to be absorbed by the LZ in the proposed configuration B (LZ loop control in Fig. 1).

It can be observed that double control loops, based on [44], regulate the active and reactive power demanded by the crane, which is provided by the FC system. In this structure, two PI controllers regulate the d and q components of the grid current in the inner control loops. The output of these PI controllers is u_d and u_q (compensators terms) allowing an independent regulation of $i_{d,AC}$ and $i_{q,AC}$, and therefore, of the active and reactive powers (see Eq. (1)). The reference values for these currents ($i_{d,AC}$ and $i_{q,AC}$) are obtained from the outer control loop, where two PI controllers regulate the active and reactive powers to their reference values.

$$m_d = \frac{2}{V_{DC}}\left(u_d - L\cdot\omega_0\cdot i_q + V_{d,AC}\right)$$
$$m_q = \frac{2}{V_{DC}}\left(u_q - L\cdot\omega_0\cdot i_d + V_{q,AC}\right) \quad (1)$$

As seen in Fig. 1, m_d and m_q are outputted from the current control loop, calculated by Eq. (1), and then transformed to the abc frame to obtain m_{abc}, which are inputted to the qZSI models (see Fig. 1).

As for D, unlike what happens with M (same control loops for both configuration), since each configuration has a different control variable, the control loops are not exactly the same. Nevertheless, in both cases, D is calculated by adding ΔD and D_0 to achieve a fast system response. The term ΔD is the output of the LZ current control loop, whereas D_0 is given

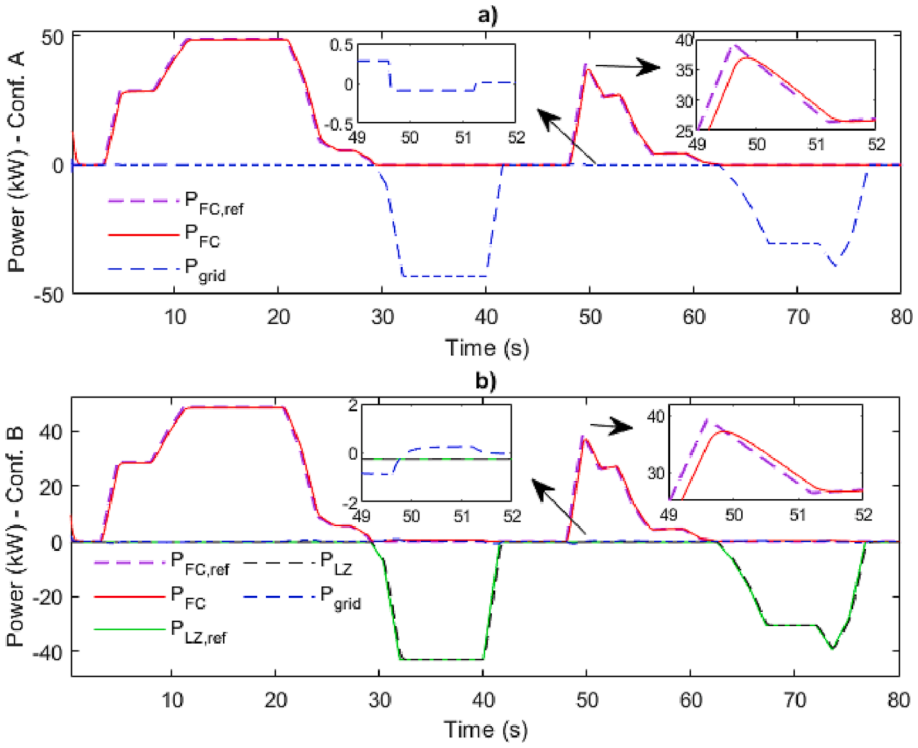

Fig. 2. A) Configuration a: fc reference power, fc power and grid power; b) configuration b: fc reference power, fc power, lz reference power, lz power and grid power.

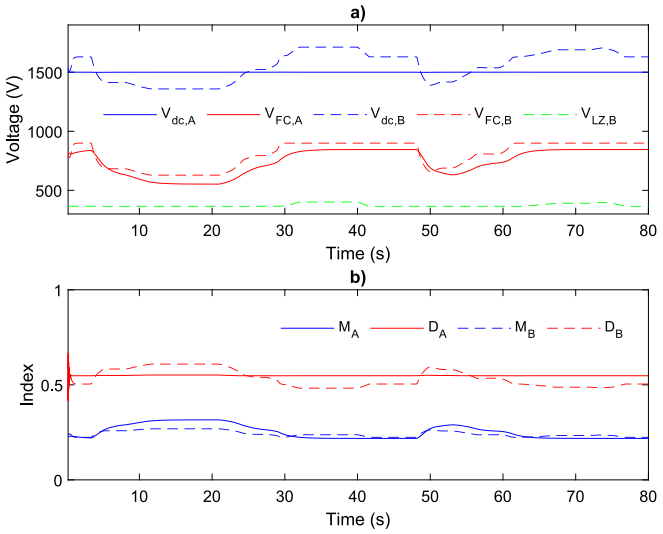

Fig. 3. A) Configuration a and b:V_{dc} and FC voltage; Configuration B: LZ voltage; b) Configuration A and B: modulation index (M) and shoot through cycle (D).

by Eq. (2). This expression derives D_0 from the input voltage of the qZSI at the nominal power of the FC (V_{FC}^{nom}), and the nominal voltage across capacitor C2, which is the nominal voltage of the LZ (V_{LZ}^{nom}). Eq. (2) provides a constant value for D_0. Subsequently, ΔD causes D to vary around D_o to control the objective variable. Fig. 1 illustrates the control loops implemented for both configurations.

$$D_0 = V_{LZ}^{nom} / \left(2 \cdot V_{LZ}^{nom} + V_{FC}^{nom}\right) \quad (2)$$

In the configuration A, D controls V_{dc}, which is set to 1500 V. In the qZSI model, V_{dc} is not a measured term. Therefore, V_{dc} has to be calculated through B and V_{FC}. In the second configuration, D controls the power to be absorbed by the LZ through a current loop control. Thus, once P_{LZ}^{ref} is set (negative values in the operation cycle of the crane), it is divided by the LZ voltage to generate the current reference. After the comparison between the reference and the measured LZ current, a PI controller generates ΔD, as shown in Fig. 1 (LZ loop control).

Results and discussion

This section shows the behavior and the technical and economic feasibility of the two new hydrogen-based configurations. The technical feasibility is evaluated through three kinds of simulations, in which the working cycle of the crane is used as the system load. To test the power flow in both configurations, and under different conditions of hydrogen level in the tank (Figs. 2-5). On the other hand, to address the economic viability of both hydrogen-based configurations, these proposals are compared, from the economic point of view, with the initial configuration (based on diesel engine) and with a full-electric configuration, where the crane is fed exclusively by the power grid (Fig. 6 and Table 2).

Technical feasibility

The technical feasibility of the hydrogen-based configuration is shown in this section. Figs. 2-4 represent the values of the main terms of the crane along the working cycle commented in Appendix A. On the hand, the importance of the LZ can be observed in Fig. 5. In this case, several working cycles are simulated until reaching a minimum level of hydrogen in the tank.

Fig. 2 shows the powers of the crane with both hydrogen-based configurations (conf. A and B) under a working cycle of the crane and with a full hydrogen tank at the beginning of the simulation. In general, the power control on each configuration responds to the specifications shown in Table 1. It can be observed in Fig. 2a and 2b that the FC generates the positive values of the curve (i.e.: the load demanded by the crane). During the periods 5–30 s and 48–62 s, and due the slow dynamic response of the FC, the grid only injects the power peaks that the

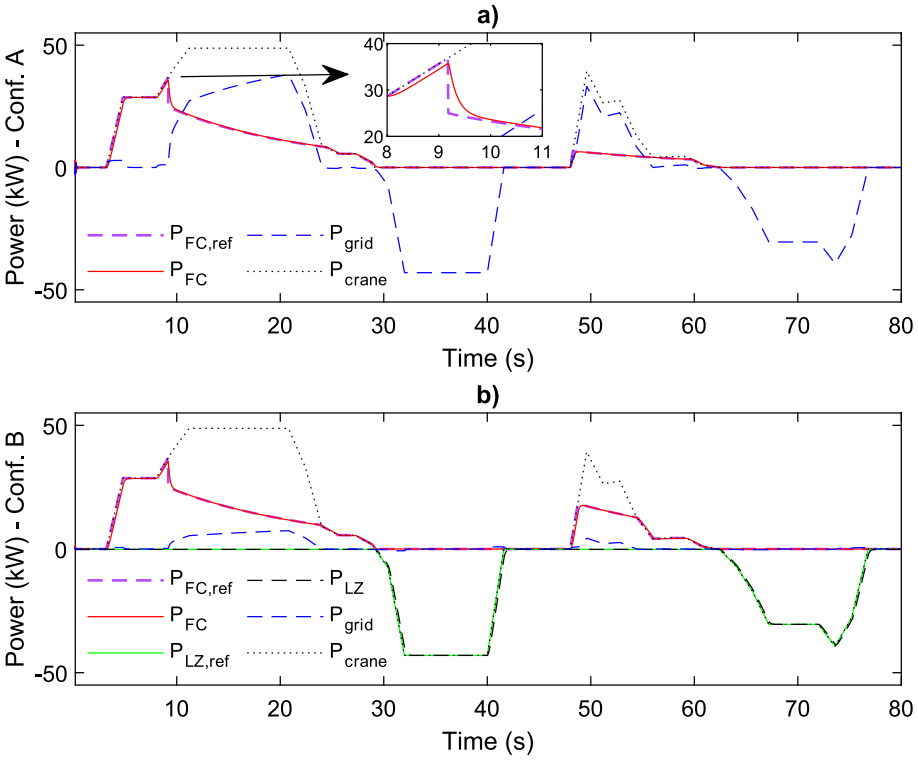

Fig.4. A) Configuration A: FC reference power, FC power and grid power; b) Configuration B: FC reference power, FC power, LZ reference power, LZ power and grid power.

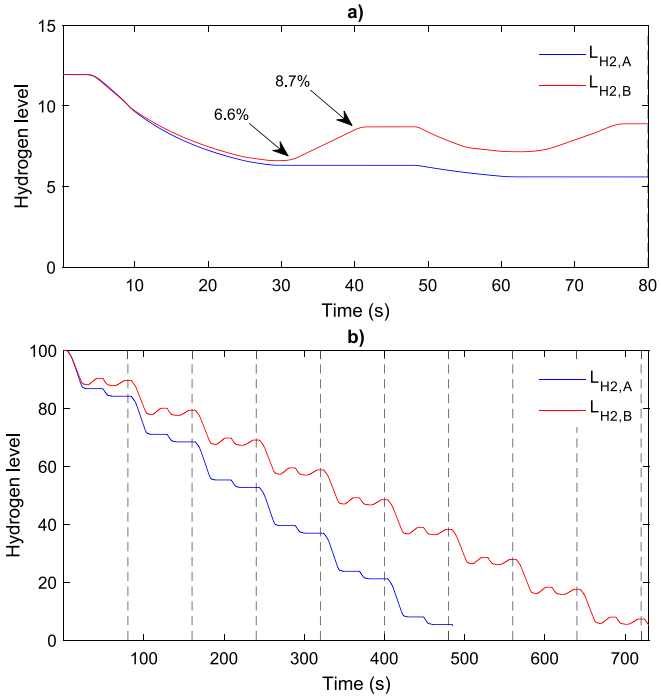

Fig. 5. Hydrogen level for both configurations: a) Simulation with initial low hydrogen level; and b) Simulation considering several working cycles.

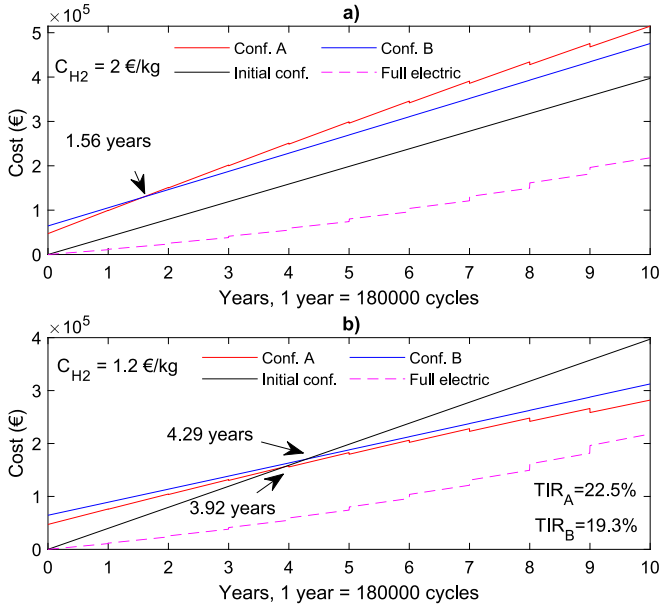

Fig. 6. A) Cost vs working cycles (current hydrogen cost situation); and b) cost vs working cycles (reduced hydrogen cost).

FC cannot generate. A zoom of this situation can be seen in Fig. 2a, although it happens in both configurations A and B. On the contrary, during the periods of negative power 30–42 s and 62–78 s (i.e.: available power), the grid absorbs this power in the configuration A, whereas, in the configuration B, the LZ produces hydrogen from this excess power. Again, in the configuration B, the grid only has to absorb the power that the LZ cannot use due to its slow dynamic response. In percentages, the grid generated just 1.6% of the power demanded by the load in the configuration A, and a 5.2% in configuration B. This small difference is due to the dynamic response of the LZ (see Fig. 2b). On the contrary, 100% of the regenerative power is absorbed by the grid in the configuration A, and only 3.5% in the configuration B.

In addition, the voltages on every point of the system, the

Table 2
Summary of costs under several situations.

	Initial conf.	Conf. A	Conf. B	Full electric
Current prices, 10 years (1.8 million cycles)	397 k€	514 k€	475 k€	218 k€
Reduced hydrogen cost. C_{H2} = 1.2 €/kg, 10 years (1.8 million cycles)	397 k€	282 k€	312 k€	218 k€
Reduced hydrogen cost. C_{H2} = 1.2 €/kg, (year to economic viability and IRR)	155 k€ (3.9 year – Conf. A) 170 k€ (4.3 year – Conf. B)	155 k€ (3.9 years IRR = 22.5%)	170 k€ (4.3 years IRR = 19.3%)	– –

modulation index *M,* and the shoot through cycle *D,* are represented in Fig. 3. More specifically, the main voltages appear in Fig. 3a and *M* and *D* in Fig. 3b. In both configurations, *M* is modified to control the FC power and to adapt the output voltage of the FC to V_{dc}. Regarding *D*, in the configuration A, this index is used to keep V_{dc} stable at 1500 V regardless the power generation of the FC. In the configuration B, this index is modified to control the power in the LZ. In this configuration, V_{dc} varies according to Eq. (A.16).

Fig. 4 is similar to Fig. 2 but corresponding to a simulation where the initial level of hydrogen in the tank was considered very low (12%). Thus, the maximum power of the FC is limited as a function of the level in the hydrogen tank according to Eq. (3), where P_{FC}^{nom} is the nominal power of the FC.

$$P_{FC}^{max} = \frac{L_{H2}}{L_{H2}^{min}} \cdot P_{FC}^{nom} \quad if \quad L_{H2} \leq L_{H2}^{min}(10\%) \tag{3}$$

In this simulation, the FC also starts generating the power demanded by the crane, but when the hydrogen level reaches a value of 10%, the FC power is limited, which makes the grid generate part of this demanded power. Fig. 5a shows the hydrogen level during this case for both configurations. Note that, during braking, the hydrogen level is recovered slightly in the configuration B due to the incorporation of the LZ. In this configuration, unlike configuration A, the hydrogen tank level increases again, from 6.6% to 8.7% (see Fig. 5a from 30 to 40 s). Hence, because of a better use of the available energy (transformed to hydrogen), configuration B is less dependent on the grid. In this sense, with the configuration A, the grid provides 55% of the demanded load, while with the configuration B, the grid supplies 41% due to the hydrogen production of the LZ.

Additionally, the hydrogen tank level corresponding to a long simulation is shown in Fig. 5b, considering several working cycles up to a total discharge of the hydrogen tank. For this simulation, in order to test the operating limits of both configurations, Eq. (3) has not been considered. The simulation ends once the FC is unable to provide any power to the system. It can be observed that, in the configuration A, the crane is able to complete six cycles before a refilling or changing of the hydrogen tank, while the crane completes nine cycles with the configuration B. This indicates that, with the same initial amount of hydrogen, the configuration B completes 50% more cycles, or said in other words, the configuration B can save up to 50% of hydrogen. This simulation is also useful to evaluate the efficiency of the hydrogen system. Thus, the ratio between the energy generated by the FC with both configurations and the available energy in the hydrogen tank provides information about the efficiency of each system. In the configuration A, an efficiency of 56.7% is registered, whereas this value increases to 81.6% in the configuration B. In the configuration A, this efficiency is directly the FC efficiency. In the case of the configuration A, this value is quite higher due to the hydrogen generation by the LZ.

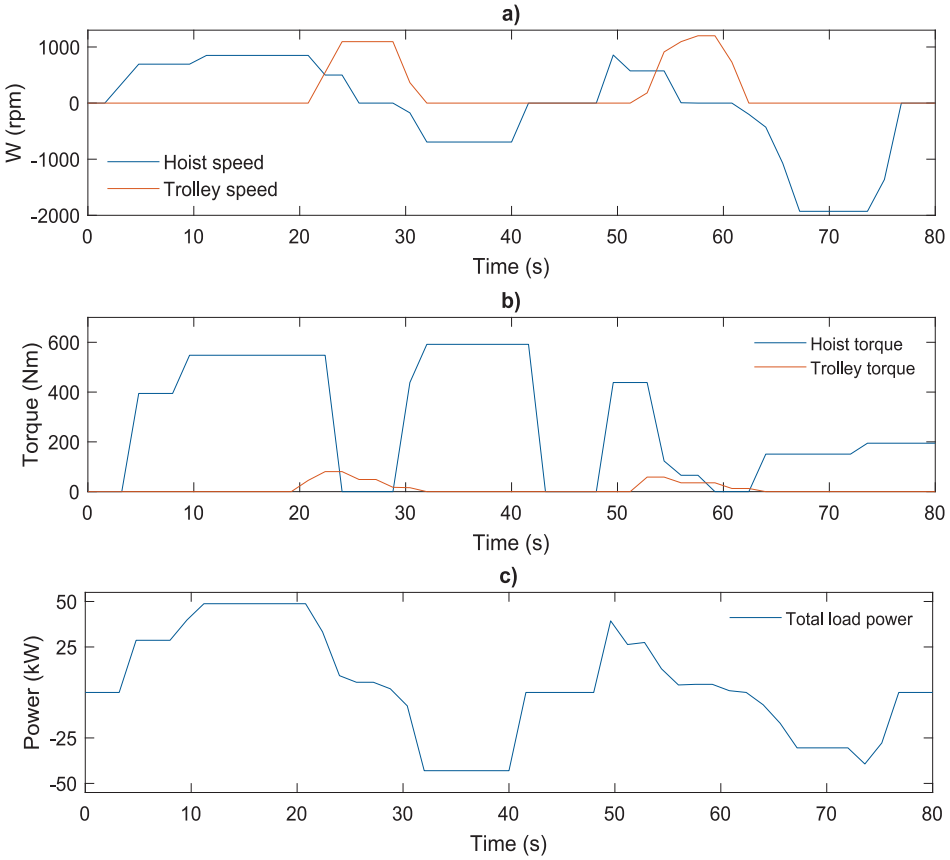

Fig. A1. Crane working cycle (hoist and trolley maneuvers): (a) motor speed; (b) torque; and (c) total load power.

Table B1
Main parameters used in the modelling and control of the configurations under study.

Parameter	Value
Fuel cell (NEDSTACK FCS 10-XXL, [46])	
Number of FC in parallel, N_{FC}	5
Number of the stacks, N_{stack}	75
FC Voltage (nominal value), V_{FC}^{nom}	625 V
FC power (nominal power), P_{FC}^{nom}	55 kW
Nominal current density.	1 A/cm^2
Fuel inlet temperature	50–60 °C
Maximum operating pressure	450 mbar
Maximum H_2 consumption	12 Nl/min
Standard of hydrogen composition	ISO 14687–2
Electrolyzer (PROTON C SERIES, C20, [47])	
Number of LZ in series, $N_{s,LZ}$	3
Number of LZ in paralel, $N_{p,LZ}$	245
LZ power (nominal voltage), V_{LZ}^{nom}	580 V
LZ power (nominal power), P_{LZ}^{nom}	100 kW
Hydrogen tank capacity, CAP_{H2}	2.25 kg
Power consumed per mass of H_2 gas produced	66.7 kWh/kg
Standard of hydrogen production	ISO 14687–2
Control specifications	
Nominal inverter input voltage (output voltage of the impedance network), V_{dc}	1500 V
Grid voltage (rms value)	400 V
Sample time	1e-4 s
PI controller gains: FC power control loop (*kp, ki*)	0.25 / 27
PI controller gains: Reactive control loop (*kp, ki*)	−2 / −200
PI controller gains: LZ power control loop (*kp, ki*)	−0.018 / −2.7
PI controller gains: i_{dq} grid control loop (*kp, ki*)	1.27 / 0.012
PI controller gains: V_{dc} control loop (*kp, ki*)	0.002 / 0.015

Economic feasibility

As previously stated, the hydrogen-based configurations, the initial (diesel-based) configuration, and the full-electric configuration (fed exclusively by the grid) are compared in this section from an economic point of view. Thus, Eq. (4) is used to calculate the utilization cost of the grid as a function of the number of working years of the crane ($N_{year} = N_{cycle}/\ N_{cycle,y}$), which depend on the number of working cycles (N_{cycle}) and the number of working cycle of the crane in a year ($N_{cycle,y}$). Moreover, the crane is able to work up to 18 h a day, which means that, taking into account a working cycle of 80 s and the maintenance periods, the crane can complete around 1.8 million cycles in ten years (expected life of the FC). The cost versus working years is represented in Fig. 6a, according to Eq. (4).

$$Cost = C_{ac} + \left(E_{abs}^{cycle} \cdot C_{grid} - E_{gen}^{cycle} \cdot C_{iny}\right) \cdot N_{cycle} + Q_{H2}^{cycle} \cdot C_{H2} \cdot N_{cycle} + E_{abs}^{cycle} \cdot Q_{die}^{kWh} \cdot C_{die} \cdot N_{cycle} \quad (4)$$

In Eq. (4), the first term (C_{ac}) corresponds to the acquisition costs. This term is null in the initial and full-electric configurations. The second term is the cost associated to the use of the grid. In this case, the available energy injected to the grid is considered as an input cost. E_{abs}^{cycle} and E_{gen}^{cycle} are the powers absorbed and generated by the system in each configuration. The third term is associated to the hydrogen consumption, only used in the hydrogen-based configurations. Q_{H2}^{cycle} is the hydrogen consumption in a cycle, and C_{H2} is the hydrogen cost in € per kilo. The last term is only applicable to the initial configuration. Q_{die}^{kWh} is the diesel consumption per unit of energy, and C_{die} is the diesel cost in € per liter.

This comparison tries to find the minimum number of N_{year} from which a new configuration (configuration A, B o full-electric) becomes economically viable (see Fig. 6). The following values have been considered: C_{ac} *(FC/LZ)* = 180 €/kW [45]; C_{ac} *(qZSI)* = 22400 €; C_{grid} = 21c€/kWh (average annual increase of 5%); C_{iny} = 15c€/kWh (average annual increase of 5%); C_{H2} = 2 €/kg [5]; C_{die} = 1.35 €/l; Q_{die}^{kWh} = 0.58 l/kWh. In addition, a reduced hydrogen cost of 1.2 €/kg has also been considered, but retaining the costs of the technology associated to it (FC and LZ). According to [3], this cost can be achieved in five years approximately, considering the current tendency.

Table 2 (first row) and Fig. 6a show the total utilization cost of the crane for the four configurations and after 10 years of operation. It is clearly observed that both hydrogen configurations are not economically feasible, and that the full-electric is the most economic configuration. Comparing both hydrogen-based configurations, it can be observed that despite the fact that the acquisition costs of configuration B are higher, after one and half year approximately, the total cost of this configuration is lower than the configuration A. Fig. 6a shows the exact cut-off point between the hydrogen-based configurations (1.56 years). Therefore, the use of the LZ in this configuration is completely justified. One of the main factors that cause the economic infeasibility of the hydrogen-based configurations is the hydrogen cost. The cost considered (2 €/kg) corresponds to a hydrogen-based synfuel cost. As it can be noted in the second row, if hydrogen was produced from renewable energy or if this cost decreased, the viability of both hydrogen-based configurations would be very different. The second row of Table 2

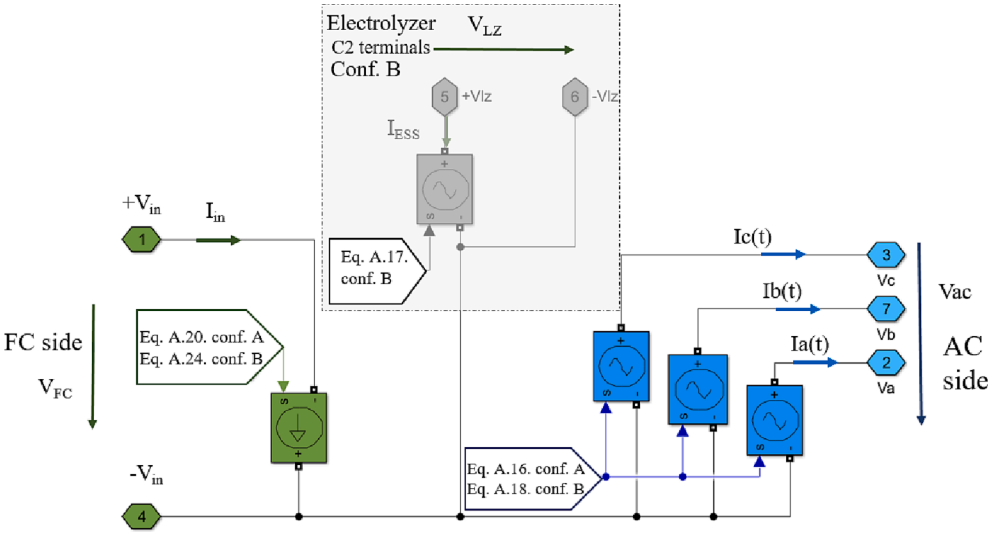

Fig. A2. Simplified model of the qZSI.

shows the total cost considering the reduced hydrogen cost of 1.2 €/kg. In this scenario, after 10 years, the hydrogen-based configurations are more profitable than the initial configuration. In either case (current and reduced hydrogen cost), full-electric version (directly connected to the grid) is still more profitable. The third row of Table 2 shows the time required for the hydrogen-based configurations to become more profitable than the initial (diesel based) and the full-electric configurations in the reduced hydrogen cost (1.2 €/kg) scenario. It can be observed (also in Fig. 6b) that the configuration A becomes more profitable than the initial configuration after 3.9 years, and the configuration B after 4.3 years approximately. Again, among all the options, the full-electric configuration is the cheapest.

On the other hand, in addition to the study previously illustrated, all companies need to evaluate the investment with any method or index before approving it. The internal return ratio (IRR) is one of the most useful metric indices to know the profitability of a potential investment. In general, it can be stated that the higher the index, the more economically viable the project is. The IRR is obtained from Eq. (5), where C_t is the net cash flow during a certain period t and calculated for the expected period of the investment.

$$C_{ac} = \sum_{t=1}^{T} \frac{C_t}{(1+IRR)^t} \tag{5}$$

Table 2 shows that, with the current situation of prices, both hydrogen-based configurations are not feasible, nevertheless, in the scenario with a reduced hydrogen cost (1.2 €/kg), these configurations obtain a quite interesting values of IRR, which give "green light" for the development of them.

Conclusions

This work presented and evaluated two new hydrogen-based configurations for a 50 kW overhead crane equipped with a qZSI. This crane is currently powered by a diesel engine and has a working cycle of 80 s.

The main innovative aspects of this work were the use of a FC as the primary power source, integrating an LZ as ESS to recover energy and produce hydrogen during braking, and the use of a qZSI that allowed the connection and control of two energy sources with a single-stage power converter, instead of the conventional two-stage power conversion with a DC-DC boost converter and a three-phase voltage source inverter. Besides, the development of a simplified model for the qZSI and the techno-economic feasibility analysis of the configurations can also be considered novelties of the work.

In the two new proposed configurations (called configurations A and B), the primary energy source was a PEM-FC, which was connected to the input of the impedance network. In the configuration A, an LZ was not considered, whereas in the configuration B, an LZ was connected in parallel with the capacitor C2 of the impedance network. Thanks to the LZ, part of the available energy during the working cycle was used to produce hydrogen. The two new configurations were evaluated under different conditions of hydrogen tank level and several consecutive 80 s-long working cycles of the crane.

The simulations proved the technological feasibility of both configurations with qZSI. This converter allowed a proper control and power flow between the components of the crane. Nevertheless, comparing these configurations, from an economic point of view, with the current implementation and with a full-electric solution, where the crane was directly connected to the grid, the results were quite different. This comparison demonstrated that the current prices, especially the hydrogen prices, are not adequate for a hydrogen-based configuration. After ten working years (expected life of the hydrogen system) none of the hydrogen configurations were more profitable than the current diesel-based configuration. Only if the hydrogen cost in €/kg was 60% less than the current price, the hydrogen configurations would be economically viable. Nonetheless, in both hydrogen cost scenarios evaluated (2 and 1.2 €/kg), the full-electric configuration was the most economical.

The main findings of the study can be summarized as follows:

- In comparison with diesel-based configuration, hydrogen is a technically viable and environmentally interesting alternative to supply power to industrial cranes.
- The current cost of hydrogen poses a significant limitation to a broader exploitation of this energy vector for electric power applications.
- A 40% reduction in the cost of hydrogen (which is considered a plausible scenario in approximately five years by some studies) would change the paradigm and make the hydrogen-based configurations more cost-effective than the initial diesel-based configuration.
- With the current hydrogen costs, the configuration with an LZ and energy recovery is preferable from an economic point of view.
- The full-electric configuration outperforms all the rest in economic terms.

After demonstrating, in this study, the technical viability of the hydrogen-based configurations with qZSI for an overhead crane, further research in the topic is desirable. Future research goes towards the integration of a second ESS (e.g.: battery or supercapacitor), that would shorten the expected time for becoming a cost-effective solution and overcoming the current limitations of the system, such as the utilization of working cycles for the crane with different length (not only 80 s) and different nominal powers; or the insertion of a prediction system for the energy management and hydrogen cost throughout the years.

CRediT authorship contribution statement

Pablo García-Triviño: Conceptualization, Formal analysis, Investigation, Methodology, Writing – original draft. **Raúl Sarrias-Mena:** Conceptualization, Formal analysis, Investigation, Methodology, Writing – original draft. **Carlos Andrés García-Vázquez:** Conceptualization, Formal analysis, Methodology, Writing – review & editing. **Francisco Llorens-Iborra:** Conceptualization, Formal analysis, Methodology, Writing – review & editing. **Higinio Sánchez-Sainz:** Conceptualization, Formal analysis, Methodology, Writing – review & editing. **Luis M. Fernández-Ramírez:** Conceptualization, Funding acquisition, Methodology, Project administration, Supervision, Writing – review & editing.

Declaration of Competing Interest

The authors declare that they have no known competing financial interests or personal relationships that could have appeared to influence the work reported in this paper.

Data availability

The authors are unable or have chosen not to specify which data has been used.

Acknowledgments

This work was partially supported by Spain's Ministerio de Ciencia, Innovación y Universidades (MCIU), Agencia Estatal de Investigación (AEI) and Fondo Europeo de Desarrollo Regional (FEDER) Unión Europea (UE) (grant number RTI2018-095720-B-C32).

Appendix A. Crane working cycle.

Currently, all electric motors of overhead cranes are commonly powered by a diesel engine. It must provide the power demanded by all movements. Moreover, the braking of the hoist and trolley motors is performed burning the available power in a resistor or through mechanical brakes. This system, despite being effective for this purpose, has a quite low efficiency from the energetic point of view, and a high dependency on the grid.

Once the operator prepares the load to be lifted, the trolley moves forward to the planned stack. The load is then hoisted and placed in the required position, and the trolley is hoisted up and returned to the initial position, where it stands for the following cycle. The load is lifted by a 68 kW motor, which can move the load at different speeds, ranging from 22 m/min under nominal load conditions, up to 44 m/min. Moreover, a 19 kW AC motor allows the trolley to moved forward and backward. Usually, in an overhead crane, gantry movement is independent of the rest of the movements. Therefore, this movement was not considered in this study. However, the power required during the gantry maneuver is significantly lower than the maximum power previously indicated (38 kW vs. 68 kW). Hence, the selected hydrogen configurations are also considered valid if this movement was considered. Fig. A.1 shows the motor speed and torque demand with a nominal load of 15 tons corresponding to the hoist and trolley movements. In addition, this figure also illustrates the total power demand of the crane during a whole cycle of 80 s.

Appendix B. Modelling of the components

Table B1 shows the most representative parameters used in the modelling and control of both configurations.

Fuel cell

PEM-FC are a feasible solution for transport and portable applications. Compared to other FC technologies, PEM-FC show a high-power density and durability, and relatively good dynamic performance. Additionally, their efficiency is higher than that of the ICE, and they do not require high operation temperatures, [10,48,49].

For the new hydrogen-based configurations of the overhead crane, a 55 kW (625 V) PEM-FC from the generic FC model of MathWorks [50], which has been tested for FC vehicles, has been selected. The model considered for the FC is the reduced model presented in [51]. The values of the most specific parameters can be found on this reference. The proposed model has already been used in high power transmission systems like tramways or RTG cranes [41,52]. Some assumptions and simplifications are considered in the reduced FC model. The most relevant are listed below:

- Hydrogen and air are ideal gases at the input.
- Hydrogen is supplied to the FC directly from a tank, and air from a compressor with a stable mass flow. No losses or dynamic behavior is modelled for the manifolds.
- The FC model does not use neither humidifier nor air-cooler. Therefore, its relative humidity is constant, and its working temperature is optimal.
- The working temperature is considered optimal, and the relative humidity constant. No air coolers or humidifiers are modelled.

The voltage of the FC (V_{FC}), as in Eq. (A.1), is the input of the qZSI. It can be derived from the Nernst's instantaneous voltage (E_{cell}) and the irreversible voltage (V_{irrev}), which is obtained by adding the activation and ohmic voltages (V_{act} and V_{ohm}, respectively). The concentration drop voltage is considered null herein.

$$V_{FC} = N_{FC}\cdot(E_{cell} - V_{irrev}) = N_{FC}\cdot(E_{cell} - (V_{act} + V_{ohm})) \tag{A.1}$$

The Nernst's voltage E_{cell} is obtained from Eq. (A.2).

$$E_{cell} = E^{0}_{cell} - k_e\cdot(T - T_{ref}) - \frac{R\cdot T}{2\cdot F} ln\left(\frac{p_{H20}}{p^{0.5}_{02}\cdot p_{H2}}\right) \tag{A.2}$$

In addition, the amount of hydrogen and oxygen reacting in the anode and cathode of the FC, respectively, is obtained from Faraday's law in Eqs. (A.3) and (A.4). Assuming a utilization factor of one, the hydrogen consumption (q^{com}_{H2}) coincides with the hydrogen that reacts.

$$q^{r}_{H2} = \frac{N_{stack}\cdot I_{FC}}{2\cdot F} \tag{A.3}$$

$$q^{r}_{O2} = \frac{N_{stack}\cdot I_{FC}}{4\cdot F} \tag{A.4}$$

where I_{FC} represents the FC current (input current of the qZSI).

The power consumed by the compressor is proportional to the input air flow (q_{air}) through the thermodynamic equation (Eq. (A.5)), where q_{air} can be obtained from Eq. (A.6) considering a relative humidity of 100%.

$$P_{com} = \frac{C_p T_{atm}}{\eta_{com}}\left[\left(\frac{p_{cat}}{p_{atm}}\right)^{(\gamma-1)/\gamma} - 1\right] q_{air} \tag{A.5}$$

$$q_{air} = \left(1 + \frac{M_v\cdot p_{sat}(T_{atm})}{M_a\cdot[p_{atm} - p_{sat}(T_{atm})]}\right)\cdot\frac{1}{x_{02}}\cdot\lambda_{O2}\cdot M_{O2}\frac{N\cdot I_{FC}}{4\cdot F} \tag{A.6}$$

The new configurations comprehend the dynamic performance of the system. In the cases when the FC cannot supply the crane with the demanded power, the grid will be responsible for compensating the difference. In this sense, a first order system in the FC current has been considered to model its dynamic response.

Electrolyzer

For the modelling of LZ in power dynamic studies, reduced linear models are a common choice for their lower complexity compared to detailed models, which results in lower computational effort, without a significant loss in accuracy for this sort of analysis [53]. A review on PEM-LZ modelling was presented in [54]. The LZ model used in the present work is based on the model B developed in [53], which has been scaled to obtain an electrolyzer of 80 kW (580 V). The LZ model consists of a controlled DC voltage source defined by Eq. (A.11). As seen, the LZ output voltage (V_{LZ}) is affected by pressure and temperature variations. This effect has been introduced in the model through the reverse voltage (V_{rev}), the internal resistance of the LZ (R_i), and the instantaneous current (I_{LZ}), as shown in Eq. (A.7) [55].

$$V_{LZ} = V_{rev}(T,p) + I_{LZ}\cdot R_i(T,p) \tag{A.7}$$

Considering temperature and pressure effects allows using this model in studies where variations of these magnitudes are plausible. Otherwise, it would be necessary to modify other parameters of the model. A closer look to Eq. (A.7) reveals the linear variation of V_{LZ} with I_{LZ} under constant pressure and temperature. The slope of this linear variation under constant operating conditions is defined by R_i. Moreover, V_{rev} represents the minimum voltage that produces a current flow in the device.

The reverse voltage e_{rev} is calculated through Eq. (A.8), where V_{rev0} is the reference value for e_{rev}. This parameter, as well as the reference pressure p_0, are defined so as to match the polarization curve of a commercially available LZ. The ideal gas constant is R, whereas T and p are temperature and pressure in the LZ, respectively.

$$e_{rev} = V_{rev0} + \frac{R\cdot T}{2\cdot F}\cdot ln\left(\frac{p}{p_0}\right) \tag{A.8}$$

The internal resistance of the LZ model is given by Eq. (A.9), where R_{i0} and T_0 are references for the internal resistance and temperature, respectively. The terms dR_t and k introduce the variation of the LZ internal resistance with temperature and pressure, respectively. The values given in [55] for these coefficients have been chosen here as a starting point, and then they have been adapted to replicate the characteristics of the commercial LZ used as a reference.

$$R_i = R_{i0} + k\cdot ln\left(\frac{p}{p_0}\right) + dR_t\cdot(T - T_0) \tag{A.9}$$

Finally, the LZ voltage is affected by the number of cells connected in series (n_c) and parallel branches (n_p) in the device. In this sense, the voltage terms in the previous equations are multiplied by n_c, whereas the current is divided by n_p.

The LZ model is completed with the calculation of the hydrogen production (q_{H2}^{pro}) through Eq. (A.10). Again, this variable depends on the operating temperature and pressure conditions through T and p, and by the amount of energy electric energy absorbed through I_{LZ} times n_c.

$$q_{H2}^{pro} = \frac{R\cdot T}{p}\cdot\frac{I_{LZ}}{2\cdot F}\cdot n_c \tag{A.10}$$

The system defined by Eqs. (A.7)-(A.10) can reproduce satisfactorily the performance of a commercial LZ in dynamic simulations of electric hybrid systems, without a relevant loss of information compared to other more detailed, and therefore, more complex and demanding models [53].

The hydrogen tank level, L_{H2} can be calculated from Eq. (A.11), where CAP_{H2} is the hydrogen tank capacity.

$$L_{H2}(100\%) = 100\cdot\left(1 - \frac{1}{CAP_{H2}}\int\left(q_{H2}^{pro} - q_{H2}^{con}\right)\cdot dt\right) \tag{A.11}$$

Simplified models of the quasi-Z-source inverter

In both hydrogen-based configurations of the overhead crane, a simplified model of the qZSI is used. This model is based on the model presented in [56], which was verified and compared with the detailed model (built with all the elements of the impedance network and switches of the inverter) by computational and real-time simulations. The simplified model consists of controlled voltage and current sources that substitute the passive elements of the impedance network, and the electronic switches of the inverter, as seen in Fig. A.2. The boost factor and the modulation index (B and m_{abc}, respectively), play a crucial role in the definition of the controlled sources.

It is important to highlight that the firing pulses of the inverter switches are not generated in the simplified models of the qZSI. Subsequently, current and voltage harmonics at the output cannot be evaluated, making this model invalid for power quality studies. On the other hand, this simplification allows increasing the time step in simulations, which reduces the computational time significantly. Additionally, the simplified model shows an acceptable accuracy when compared to the detailed model of the qZSI in terms of the dynamic response. These advantages make the simplified model a pertinent choice for this work, where the main aim is to evaluate the energy management and power flows in the system.

In both configurations (with or without LZ), B is the voltage gain between the input and the output of the impedance network (namely V_{in} and V_{dc}, respectively). Besides, the output AC voltage of the inverter and V_{dc} are related through the modulating index m_{abc}, as defined by Eqs. (A.12) and (A.13).

$$V_{dc} = B\cdot V_{in} = \frac{1}{1-2D}\cdot V_{in} \tag{A.12}$$

$$V_a = \frac{1}{\sqrt{3}}(V_{dc} \cdot m_a)$$
$$V_b = \frac{1}{\sqrt{3}}(V_{dc} \cdot m_b) \quad (A.13)$$
$$V_c = \frac{1}{\sqrt{3}}(V_{dc} \cdot m_c)$$

where D represents the shoot-through period.

Finally, the voltage across capacitor C2 (V_{C2}) can be derived from V_{in} through Eq. (A.14).

$$V_{C2} = V_{in} \cdot B \cdot D \quad (A.14)$$

In the simplified model of the quasi-Z-source inverter (configuration A, without electrolyzer) a controlled current source and three controlled voltage sources in the DC and AC sides, respectively, model the response of the qZSI. Since there is not any element connected in parallel with C2, V_{dc} is not considered, and therefore its value has to be calculated from V_{in} and the boost factor B. Thus, a direct relation (see Eq. (A.19)) between the input (V_{in}) and the output voltages of the qZSI can be found substituting V_{dc} from Eq. (A.16) into Eq. (A.17).

$$V_a = \frac{B}{\sqrt{3}}(V_{in} \cdot m_a)$$
$$V_b = \frac{B}{\sqrt{3}}(V_{in} \cdot m_b) \quad (A.15)$$
$$V_c = \frac{B}{\sqrt{3}}(V_{in} \cdot m_c)$$

Moreover, using the power balance principle, Eq. (A.16) is obtained:

$$V_{in} I_{in} = [V_a I_a + V_b I_b + V_c I_c] \quad (A.16)$$

In the previous equation, if $V_a(t)$, $V_b(t)$ and $V_c(t)$ are replaced by Eq. (A.15), the value of the input current into this model is obtained.

$$I_{in} = \frac{B}{\sqrt{3}}[I_a \cdot m_a + I_b \cdot m_b + I_c \cdot m_c] \quad (A.17)$$

Eqs. (A.15) and (A.17) show that the controlled current source at the input, and the controlled voltage sources at the output of the model depend on B and m_{abc}.

In the simplifed model of the quasi-Z-source inverter with electrolyzer (configuration B), the qZSI with LZ model includes an additional controlled voltage source that simulates the terminals of capacitor C2, apart from the controlled current and voltage sources that also appeared in the configuration A. Thus, as observed in Fig. 1, the LZ is connected to the capacitor C2. A scheme of the controlled sources that compose the qZSI with LZ is shown in Fig. A.2. In this configuration, the relation between the input voltage and the AC voltage is the same as in the configuration without LZ. Hence, Eq. (A.15) is still valid.

Proceeding similarly to the previous model, the controlled current source in the FC side of the qZSI is calculated from the power balance principle ($P_{grid} = P_{FC} + P_{LZ}$) applied on the FC terminals (V_{in}).

$$\begin{aligned} P_{grid} &= I_a \cdot V_a + I_b \cdot V_b + I_c \cdot V_c \\ P_{in} &= V_{in} \cdot I_{in} \\ P_{LZ} &= V_{C2} \cdot I_{LZ} = V_{LZ} \cdot I_{LZ} \end{aligned} \quad (A.18)$$

Eq. (A.18) derived from the FC side are as follows, considering that V_{LZ} is equal to $V_{in}B \cdot D$ [42].

$$\begin{aligned} P_{grid} &= \frac{V_{in}}{\sqrt{3}} \cdot B \cdot (I_a \cdot m_a + I_b \cdot m_b + I_c \cdot m_c) \\ P_{in} &= V_{in} \cdot I_{in} \\ P_{LZ} &= V_{in} \cdot B \cdot D \cdot I_{LZ} \end{aligned} \quad (A.19)$$

Finally, the input current of the qZSI can be obtained from the power balance. Note that P_{LZ} is always negative.

$$I_{in} = \frac{1}{\sqrt{3}} \cdot B \cdot (I_a \cdot m_a + I_b \cdot m_b + I_c \cdot m_c) - B \cdot D \cdot I_{LZ}$$

where

$$I_a \cdot m_a + I_b \cdot m_b + I_c \cdot m_c \rightarrow m_{abc} \cdot I_{abc} \quad (A.20)$$

$$I_{in} = \frac{1}{\sqrt{3}} \cdot B \cdot m_{abc} \cdot I_{abc} - B \cdot D \cdot I_{LZ} \quad (A.21)$$

where $I_{acb}(t)$ is the AC current, I_{ESS} is the ESS current, and I_{in} is the FC current.

Power demand

A simple but effective way to model the power demanded by the crane is by means of controlled current sources, whose value depend on the AC voltage measurement and the power of the working cycle represented in Fig. A.1. Thus, once the AC voltage is measured and converted to the dq

reference frame, the current associated to the power demand can be calculated from Eq. (A.21). Finally, if I_d and I_q are expressed in the *abc* reference frame, the sinusoidal signal of each controlled current source is obtained.

$$P = \frac{3}{2}\left(V_d \cdot I_d + V_q \cdot I_q + V_0 \cdot I_0\right)$$
$$Q = \frac{3}{2}\left(V_q \cdot I_d - V_d \cdot I_q\right) \tag{A.22}$$

References

[1] International Energy Agency (IEA). World Energy Outlook 2022; November, 2022.
[2] BP Statistical Review of World Energy, 71st edition; June, 2022.
[3] Parra D, Valverde L, Pino FJ, Patel MK. A review on the role, cost and value of hydrogen energy systems for deep decarbonisation. Renew Sustain Energy Rev 2019;101:279–94. https://doi.org/10.1016/j.rser.2018.11.010.
[4] Faisal M, Hannan MA, Ker PJ, Hussain A, Bin Mansor M, Blaabjerg F. Review of energy storage system technologies in microgrid applications: Issues and challenges. IEEE Access 2018;6:35143–64. https://doi.org/10.1109/ACCESS.2018.2841407.
[5] Hydrogen Council, Path to hydrogen competitiveness: a cost perspective, (2020) 88. www.hydrogencouncil.com.
[6] Das V, Padmanaban S, Venkitusamy K, Selvamuthukumaran R, Blaabjerg F, Siano P. Recent advances and challenges of fuel cell based power system architectures and control – A review. Renew Sustain Energy Rev 2017;73:10–8. https://doi.org/10.1016/j.rser.2017.01.148.
[7] Su-ungkavatin P, Tiruta-Barna L, Hamelin L. Biofuels, electrofuels, electric or hydrogen?: A review of current and emerging sustainable aviation systems. Prog Energy Combust Sci 2023;96:101073. https://doi.org/10.1016/j.pecs.2023.101073.
[8] Aguilar P, Groß B. Battery electric vehicles and fuel cell electric vehicles, an analysis of alternative powertrains as a mean to decarbonize the transport sector. Sustain Energy Technol Assessments 2022;53:102624. https://doi.org/10.1016/j.seta.2022.102624.
[9] Kim Y, Han J, Yu S. Establishment of energy management strategy of 50 kW PEMFC hybrid system. Energy Rep 2023;9:2745–56. https://doi.org/10.1016/j.egyr.2023.01.096.
[10] Soumeur MA, Gasbaoui B, Abdelkhalek O, Ghouili J, Toumi T, Chakar A. Comparative study of energy management strategies for hybrid proton exchange membrane fuel cell four wheel drive electric vehicle. J Power Sources 2020;462:228167. https://doi.org/10.1016/j.jpowsour.2020.228167.
[11] Chen PC. Configuration of solar-hydrogen mild hybrid fuel cell power systems for electric vehicles. J Power Sources 2012;201:243–52. https://doi.org/10.1016/j.jpowsour.2011.10.126.
[12] Wu P, Bucknall R. Hybrid fuel cell and battery propulsion system modelling and multi-objective optimisation for a coastal ferry. Int J Hydrogen Energy 2020;45:3193–208. https://doi.org/10.1016/j.ijhydene.2019.11.152.
[13] Attemene NS, Agbli KS, Fofana S, Hissel D. Optimal sizing of a wind, fuel cell, electrolyzer, battery and supercapacitor system for off-grid applications. Int J Hydrogen Energy 2020;45:5512–25. https://doi.org/10.1016/j.ijhydene.2019.05.212.
[14] Dash V, Bajpai P. Power management control strategy for a stand-alone solar photovoltaic-fuel cell-battery hybrid system. Sustain Energy Technol Assessments 2015;9:68–80. https://doi.org/10.1016/j.seta.2014.10.001.
[15] Alam M, Kumar K, Verma S, Dutta V. Renewable sources based DC microgrid using hydrogen energy storage: Modelling and experimental analysis. Sustain Energy Technol Assessments 2020;42:100840. https://doi.org/10.1016/j.seta.2020.100840.
[16] Xu X, Hu W, Cao D, Huang Q, Liu W, Jacobson MZ, et al. Optimal operational strategy for an offgrid hybrid hydrogen/electricity refueling station powered by solar photovoltaics. J Power Sources 2020;451:227810. https://doi.org/10.1016/j.jpowsour.2020.227810.
[17] Al-Ghussain L, Ahmad AD, Abubaker AM, Hovi K, M.A., A. Hassan, Annuk.. Techno-economic feasibility of hybrid PV/wind/battery/thermal storage trigeneration system: Toward 100% energy independency and green hydrogen production. Energy Rep 2023;9:752–72. https://doi.org/10.1016/j.egyr.2022.12.034.
[18] Hafsi O, Abdelkhalek O, Mekhilef S, Soumeur MA, Hartani MA, Chakar A. Integration of hydrogen technology and energy management comparison for DC-Microgrid including renewable energies and energy storage system. Sustain Energy Technol Assessments 2022;52:102121. https://doi.org/10.1016/j.seta.2022.102121.
[19] Wang J, An Q, Zhao Y, Pan G, Song J, Hu Q, et al. Role of electrolytic hydrogen in smart city decarbonization in China. Appl Energy 2023;336:120699. https://doi.org/10.1016/j.apenergy.2023.120699.
[20] Dermühl S, Riedel U. A comparison of the most promising low-carbon hydrogen production technologies. Fuel 2023;340:127478. https://doi.org/10.1016/j.fuel.2023.127478.
[21] Guilbert D, Yodwong B, Kaewmanee W, Phattanasak M. Power converters for hybrid renewable energy systems with hydrogen buffer storage: A short review. In: 6th IEEE Int. Conf. Smart Grid, IcSmartGrids 2018 (2019) 28–33. https://doi.org/10.1109/ISGWCP.2018.8634562.
[22] İnci M, Türksoy Ö. Review of fuel cells to grid interface: Configurations, technical challenges and trends. J Clean Prod 2019;213:1353–70. https://doi.org/10.1016/j.jclepro.2018.12.281.
[23] Yu X, Starke MR, Tolbert LM, Ozpineci B. Fuel cell power conditioning for electric power applications: a summary. IET Electr Power Appl 2007;1:643–56. https://doi.org/10.1049/iet-epa.
[24] Jung JW, Keyhani A. Control of a fuel cell based Z-source converter. IEEE Trans Energy Convers 2007;22:467–76. https://doi.org/10.1109/TEC.2006.874232.
[25] Gitizadeh M, Nayeripour M, Akrami A. Maximum constant boost control for QZSI in a fuel cell system. In: 2012 2nd Iran. Conf. Renew. Energy Distrib. Gener. ICREDG 2012. (2012) 7–11. https://doi.org/10.1109/ICREDG.2012.6190473.
[26] Jalakas T, Roasto I, Vinnikov D, Agabus H. Novel power conditioning system for residential fuel cell power plants. In: Proc. - 2012 3rd IEEE Int. Symp. Power Electron. Distrib. Gener. Syst.m in: PEDG 2012. (2012) 578–585. https://doi.org/10.1109/PEDG.2012.6254060.
[27] Rekha Y, Christopher IW, Jamuna V. Fuel Cell Based Sl Quasi Z-Source Inverter for Motor Drive. In: 5th Int. Conf. Electr. Energy Syst. ICEES 2019. (2019) 1-6. https://doi.org/10.1109/ICEES.2019.8719296.
[28] Alasali F, Luque A, Mayer R, Holderbaum W. A comparative study of energy storage systems and active front ends for networks of two electrified RTG cranes. Energies 2019;12(9):1771. https://doi.org/10.3390/en12091771.
[29] Karam A, Eltawil A, Reinau KH. Energy-efficient and integrated allocation of berths, quay cranes, and internal trucks in container terminals. Sustain 2020;12(8):3202. https://doi.org/10.3390/SU12083202.
[30] Liu A, Liu H, Tsai SB, Lu H, Zhang X, Wang J. Using a hybrid model on joint scheduling of berths and quay cranes-from a sustainable perspective. Sustain 2018;10(6):1959. https://doi.org/10.3390/su10061959.
[31] Antonelli M, Ceraolo M, Desideri U, Lutzemberger G, Sani L. Hybridization of rubber tired gantry (RTG) cranes. J Energy Storage 2017;12:186–95. https://doi.org/10.1016/j.est.2017.05.004.
[32] Vlahopoulos D, Bouhouras AS. Solution for RTG crane power supply with the use of a hybrid energy storage system based on literature review. Sustain Energy Technol Assessments 2022;52:102351. https://doi.org/10.1016/j.seta.2022.102351.
[33] Corral-Vega PJ, Fernández-Ramírez LM, García-Triviño P. Hybrid powertrain, energy management system and techno-economic assessment of rubber tyre gantry crane powered by diesel-electric generator and supercapacitor energy storage system. J Power Sources 2019;412:311–20. https://doi.org/10.1016/j.jpowsour.2018.11.027.
[34] Alasali F, Haben S, Holderbaum W. Stochastic optimal energy management system for RTG cranes network using genetic algorithm and ensemble forecasts. J Energy Storage 2019;24:100759. https://doi.org/10.1016/j.est.2019.100759.
[35] Bolonne SRA, Chandima DP. Sizing an energy system for hybrid li-ion battery-supercapacitor RTG cranes based on state machine energy controller. IEEE Access 2019;7:71209–20. https://doi.org/10.1109/ACCESS.2019.2919345.
[36] Zhao N, Schofield N, Niu W. Energy storage system for a port crane hybrid power-train. IEEE Trans Transp Electrif 2016;2:480–92. https://doi.org/10.1109/TTE.2016.2562360.
[37] Kusakana K. Optimal energy management of a retrofitted Rubber Tyred Gantry Crane with energy recovery capabilities. J Energy Storage 2021;42:103050. https://doi.org/10.1016/j.est.2021.103050.
[38] Anton Bolonne SR, Chandima DP. Narrow band state of charge (SoC) control strategy for hybrid container cranes. Energies 2019;12(4):743. https://doi.org/10.3390/en12040743.
[39] Chen D, Niu W, Gu W, Schofield N. Game-based energy management method for hybrid RTG cranes. Energies 2019;12(18):3589. https://doi.org/10.3390/en12183589.
[40] Baizura N, Su C, Member S, Zhaoxia X, Vasquez JC, Member S, et al. Energy Harvesting From Harbor Cranes With Flywheel Energy Storage Systems. IEEE Trans Ind Appl 2019;55:3354–64. https://doi.org/10.1109/TIA.2019.2910495.
[41] Corral-Vega PJ, García-Triviño P, Fernández-Ramírez LM. Design, modelling, control and techno-economic evaluation of a fuel cell/supercapacitors powered container crane. Energy 2019;186:115863. https://doi.org/10.1016/j.energy.2019.115863.
[42] Liu Y, Ge B, Abu-Rub H, Peng FZ. Overview of space vector modulations for three-phase Z-Source/quasi-z- source inverters. IEEE Trans Power Electron 2014;29:2098–108. https://doi.org/10.1109/TPEL.2013.2269539.
[43] Zheng Peng Fang. Z-source inverter. IEEE Trans Ind Appl 2003;39:504–10.
[44] Yazdani A, Iravani R. Voltage-sourced converters in power systems: modeling, control, and applications. Hoboken, New Jersey: John Wiley & Sons Inc.; 2010.
[45] Marcinkoski J, Spendelow J, Wilson A, Papageorgopoulos D, Reviewed P, Ahluwalia R, et al. DOE Hydrogen and Fuel Cells Program Record, DOE Hydrog.

Fuel Cells Progr Rec Rec (2015) 15015. https://www.hydrogen.energy.gov/pdfs/15015_fuel_cell_system_cost_2015.pdf.
[46] NEDSTACK FCS 10-XXL Stack specifications and operating conditions Appearance impression 2022. 9-10. https://nedstack.com/sites/default/files/2022-07/nedstack-fcs-10-xxl-gen-2.9-datasheet-rev01.pdf.
[47] PROTON. Systems HG. C Series, Technical Specifications. 2018. 1-2. https://www.protonenergy.com/sites/default/files/2017-07/PD-0600-0068-rev%20F.pdf.
[48] Xie C, Ogden JM, Quan S, Chen Q. Optimal power management for fuel cell-battery full hybrid powertrain on a test station. Int J Electr Power Energy Syst 2013;53:307–20. https://doi.org/10.1016/j.ijepes.2013.05.016.
[49] Huang CN, Chen YS. Design of magnetic flywheel control for performance improvement of fuel cells used in vehicles. Energy 2017;118:840–52. https://doi.org/10.1016/j.energy.2016.10.112.
[50] Simscape TM. Reference. Natick, MA: Hydro-Québec and the MathWorks Inc; 2020.
[51] Pukrushpan JT, Stefanopoulou AG, Peng H. Control of fuel cell power systems: principles, modeling, analysis and feedback design. London: Springer Science & Business Media; 2004.
[52] Garcia P, Fernández LM, Garcia CA, Jurado F. Comparative Study of PEM Fuel Cell Models for Integration in Propulsion Systems of Urban Public Transport. Fuel Cells 2010;10:1024–39. https://doi.org/10.1002/fuce.201000002.
[53] Sarrias-Mena R, Fernández-Ramírez LM, García-Vázquez CA, Jurado F. Electrolyzer models for hydrogen production from wind energy systems. Int J Hydrogen Energy 2015;40:2927–38. https://doi.org/10.1016/j.ijhydene.2014.12.125.
[54] Falcão DS, Pinto AMFR. A review on PEM electrolyzer modelling: Guidelines for beginners. J Clean Prod 2020;261:121184. https://doi.org/10.1016/j.jclepro.2020.121184.
[55] Atlam O, Kolhe M. Equivalent electrical model for a proton exchange membrane (PEM) electrolyser. Energy Convers Manag 2011;52:2952–7. https://doi.org/10.1016/j.enconman.2011.04.007.
[56] de Oliveira-Assis L, Soares-Ramos EPP, Sarrias-Mena R, García-Triviño P, González-Rivera E, Sánchez-Sainz H, et al. Simplified model of battery energy-stored quasi-Z-source inverter-based photovoltaic power plant with Twofold energy management system. Energy 2022;244. https://doi.org/10.1016/j.energy.2021.122563.